

## Impact of PEHD plates: Experimental tests and numerical simulations

**Arild Holm Clausen, arild.clausen@ntnu.no**

CRI-SIMLab, Dept. of Structural Engineering, Norwegian University of Science and Technology (NTNU), Trondheim, Norway

**Rafael Traldi Moura, rafael.moura@poli.usp.br**

**Marcílio Alves, maralves@usp.br**

Group of Solid Mechanics and Structural Impact, University of São Paulo, Brazil

**Magnus Langseth, magnus.langseth@ntnu.no**

CRI-SIMLab, Dept. of Structural Engineering, Norwegian University of Science and Technology (NTNU), Trondheim, Norway

**Mario Polanco-Loria, mario.polanco-loria@sintef.no**

**Torodd Berstad, torodd.berstad@sintef.no**

CRI-SIMLab / SINTEF Materials & Chemistry, Trondheim, Norway

**Odd Sture Hopperstad, odd.hopperstad@ntnu.no**

CRI-SIMLab, Dept. of Structural Engineering, Norwegian University of Science and Technology (NTNU), Trondheim, Norway

**Abstract.** *This paper compares experimental results from quasi-static and dynamic tests on plates made of PEHD with predictions from numerical simulations, employing a recently developed constitutive model for thermoplastics. In order to calibrate the 10 coefficients of the model, quasi-static and dynamic material tests were also carried out. The constitutive model assumes that the resistance of the thermoplastic consists of two main parts: (A) a hyperelastic-viscoplastic response due to intermolecular resistance, and (B) an entropic hyperelastic response due to re-orientation of molecular chains. Important ingredients of the material model are a Neo-Hookean model describing the initial elasticity, Raghava's yield criterion, a non-associated Raghava-like flow rule, and Anand's model representing the entropic elasticity. It is implemented as a user-defined model in LS-DYNA. Considering a PEHD material, the coefficients of the model were calibrated from quasi-static tests in tension and compression, and dynamic compression tests applying a split-Hopkinson pressure bar. Further, quasi-static and dynamic tests were carried out on plates made of the same PEHD material. The plate tests were modelled in LS-DYNA, applying the calibrated constitutive model and four-node axisymmetric elements. The force-displacement curves found from the numerical analyses show reasonable agreement with the results from the laboratory tests..*

**Keywords:** *Thermoplastic, Constitutive model, Material tests, Impact tests, LS-DYNA*

### 1. INTRODUCTION

The increase in demand and use of polymers has been much larger than it has been for other classes of materials (metals, concrete, wood) during the last decades (Ehrenstein, 2001). The underlying reason for this growth is that polymers have several attractive properties. They are cheap, easy to form, have low density, they may be very ductile, and also, depending on additives and environment, be rather durable. In particular, polymers may have excellent energy absorption characteristics. Therefore, polymers are promising for use in many applications where other materials, e.g. metals, have been the common choice so far.

There are three main groups of polymers: Thermoplastics, thermosets and elastomers. All of them consist of long molecule chains with carbon atoms in the „backbone“. The bonding structure is, however, slightly different for the three groups. Thermoplastics have only weak van der Waals bonds between neighbour chains, giving a rather flexible structure facilitating large plastic deformations caused by relative sliding between the chains. On the other hand, intermolecular covalent bonds, or cross-links, are present for thermosets and elastomers. These cross-links imply a „memory effect“, ensuring that thermosets and elastomers behave elastic under most circumstances. Their strength and stiffness properties are different, however. While the latter group has approximately 1 cross-link connection per 1000 atoms of the main molecule chain, there is a considerably higher cross-link density in thermosets, may be 1 for every 20 atom in the backbone chain (Ehrenstein, 2001).

Thus, the difference in molecular structure has consequences for the behaviour of the polymer at hand, and also for the availability of material models for use in commercial finite element codes. While there exists rather accurate models for thermosets and elastomers, Du Bois et al. (2006) claimed that the present models for thermoplastics still called for further improvements. Generally speaking, a material model for thermoplastics should be capable of handling large temperature and strain-rate effects, deformation-induced anisotropy, viscosity, and also other commonly observed features. Certainly, it is challenging to develop a material model which covers most of these phenomena, yet has calibrations procedures which are sufficiently user friendly for industrial applications.

This paper applies a recently developed constitutive model for thermoplastics proposed by Polanco-Loria et al. (2009). The model is implemented as a user-defined material model in LS-DYNA (2007). It involves 10 coefficients which are determined from material tests in uniaxial tension and compression on a PEHD material. Subsequently, the calibrated model is employed in FEM simulations of plates made of the same material, and the numerical predictions are compared with the experimental results.

## 2. OUTLINE OF CONSTITUTIVE MODEL

### 2.1. Overview

Figure 1 summarises the main constituents of the constitutive model proposed by Polanco-Loria et al. (2009). The material response is assumed to have two Parts A and B. They represent the intermolecular and intramolecular strength, respectively. Parts A and B are kinematically described by the same deformation gradient  $\mathbf{F}$ , i.e.  $\mathbf{F} = \mathbf{F}_A = \mathbf{F}_B$ . The Cauchy stress tensor is obtained by summing the contributions of Parts A and B, i.e.  $\boldsymbol{\sigma} = \boldsymbol{\sigma}_A + \boldsymbol{\sigma}_B$ .

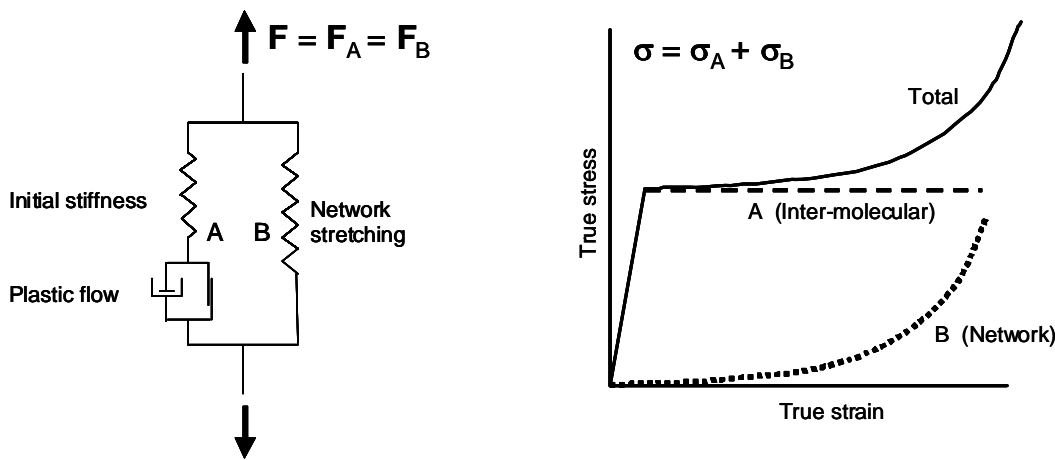


Figure 1. Proposed constitutive model with inter-molecular (A) and intra-molecular (B) contributions.

### 2.2. Part A – Inter-molecular resistance

The deformation gradient  $\mathbf{F}_A$  is decomposed into elastic and plastic parts, i.e.  $\mathbf{F}_A = \mathbf{F}_A^e \cdot \mathbf{F}_A^p$ . In a similar manner, the Jacobian  $J_A$  of Part A, representing the volume change, is decomposed as  $J_A = \det \mathbf{F}_A = J_A^e J_A^p = J$ . A compressible Neo-Hookean material is chosen for the elastic part of the deformation. Thus, the Cauchy stress tensor  $\boldsymbol{\sigma}_A$  reads

$$\boldsymbol{\sigma}_A = \frac{1}{J} (\lambda_0 \ln J_A^e \mathbf{I} + \mu_0 [\mathbf{B}_A^e - \mathbf{I}])$$

where  $\lambda_0$  and  $\mu_0$  are the classical Lamé constants of the linearized theory,  $\mathbf{B}_A^e = \mathbf{F}_A^e \cdot (\mathbf{F}_A^e)^T$  is the elastic left Cauchy-Green deformation tensor, and  $\mathbf{I}$  is the second order unit tensor. The coefficients  $\lambda_0$  and  $\mu_0$  may alternatively be expressed as functions of Young's modulus  $E_0$  and Poisson's ratio  $\nu_0$ .

The yield criterion is assumed in the form  $f_A = \bar{\sigma}_A - \sigma_T = 0$ , where  $\sigma_T$  is the yield stress in uniaxial tension. The equivalent stress  $\bar{\sigma}_A$  accounts for the pressure-sensitive behaviour, commonly observed in polymeric materials, and it is defined according to Raghava et al. (1973), viz.

$$\bar{\sigma}_A = \frac{(\alpha - 1)I_{1A} + \sqrt{(\alpha - 1)^2 I_{1A}^2 + 12\alpha J_{2A}}}{2\alpha}$$

The material parameter  $\alpha = \sigma_C / \sigma_T \geq 1$  describes the pressure sensitivity, where  $\sigma_C$  is the uniaxial compressive yield strength of the material, and  $I_{1A}$  and  $J_{2A}$  are stress invariants related to respectively the total and the deviatoric

Cauchy stress tensor. It is noted that the equivalent stress  $\bar{\sigma}_A$  is equal to the von Mises – equivalent stress  $\bar{\sigma} = \sqrt{3J_2}$  when  $\alpha = 1$ , i.e.  $\sigma_C = \sigma_T$ .

During the introductory evaluation of the model, it turned out that an associated flow rule predicted unrealistic large volumetric plastic strains. In order to control this plastic dilatation, a non-associated flow rule was introduced. A Raghava-like plastic potential  $g_A$  was chosen, reading

$$g_A = \frac{(\beta-1)I_{1A} + \sqrt{(\beta-1)^2 I_{1A}^2 + 12\beta J_{2A}}}{2\beta} \geq 0$$

where the material parameter  $\beta \geq 1$  controls the volumetric plastic strain. Isochoric plastic behaviour, preserving the volume, is obtained in the special case of  $\beta = 1$ .

Finally, the flow rule gives the plastic rate-of-deformation tensor as  $\mathbf{D}_A^p = \dot{\bar{\epsilon}}_A^p \partial g_A / \partial \boldsymbol{\sigma}_A$ , where the equivalent plastic strain rate is chosen as

$$\dot{\bar{\epsilon}}_A^p = \begin{cases} 0 & \text{if } f_A \leq 0 \\ \dot{\bar{\epsilon}}_{0A} \left\{ \exp \left[ \frac{1}{C} \left( \frac{\bar{\sigma}_A}{\sigma_T} - 1 \right) \right] - 1 \right\} & \text{if } f_A > 0 \end{cases}$$

The two coefficients  $C$  and  $\dot{\bar{\epsilon}}_{0A}$  are easy to identify from uniaxial strain-rate tests.

### 2.3. Part B – Intra-molecular resistance

The deformation gradient  $\mathbf{F}_B$ , see

Figure 1, represents the network orientation and it is assumed that the network resistance is hyperelastic. Following Anand (1996), the Cauchy stress-stretch relation is given as

$$\boldsymbol{\sigma}_B = \frac{1}{J} \left[ \frac{C_R}{3} \frac{\bar{\lambda}_L}{\bar{\lambda}} \mathcal{L}^{-1} \left( \frac{\bar{\lambda}}{\bar{\lambda}_L} \right) (\mathbf{B}_B^* - \bar{\lambda}^2 \mathbf{I}) + \kappa (\ln J) \mathbf{I} \right]$$

where the Jacobian  $J = J_B = \det \mathbf{F}$ , and  $\mathcal{L}^{-1}$  is the inverse function of the Langevin function defined as  $\mathcal{L}(\beta) = \coth \beta - 1/\beta$ . Further,  $\mathbf{B}_B^* = \mathbf{F}_B^* \cdot (\mathbf{F}_B^*)^T$  is the distortional left Cauchy-Green deformation tensor, where  $\mathbf{F}_B^* = J_B^{-1/3} \mathbf{F}_B$  denotes the distortional part of  $\mathbf{F}_B$ , and the effective distortional stretch is  $\bar{\lambda} = \sqrt{\text{tr}(\mathbf{B}_B^*)/3}$ . There are three constitutive parameters describing the intra-molecular resistance:  $C_R$  is the initial elastic modulus of Part B;  $\bar{\lambda}_L$  is the locking stretch; and  $\kappa$  is a bulk modulus.

## 3. MATERIAL TESTS

### 3.1. Quasi-static tests

PEHD plates measuring 2000mm x 1000mm were acquired from the German company Simona. The plates had thickness 5mm or 10mm. Square plates 600mm x 600mm intended for use in the impact tests were cut from the delivered plates. Further, uniaxial low-rate material tests in tension and compression were carried out on samples machined from a 10mm thick plate. The tests were performed at respectively two and three different, yet quasi-static, rates as described by Moura et al. (2009a).

A major challenge associated with material testing of ductile polymers is that they experience cold drawing in tension, meaning that a neck evolves along the whole gauge length of the sample before it eventually ruptures at a very large deformation. This means that an extensometer, which assumes a homogenous deformation field between the two knives, is not an adequate measurement tool. Also, different to metals, many polymers are susceptible to volume changes during plastic deformation. The practical consequence is that measurements of transverse strains are required in order to determine true stress. Therefore, we employed the Digital Image Correlation (DIC) technique in all tension and compression tests to facilitate in-plane full-field measurements and a subsequent deduction of true stress-strain curves.

Figure 2a shows quasi-static test results obtained in the extrusion direction of the plate material. Two replicate tests were carried out when determining the true stress-strain curve at strain rate  $10^{-3} \text{ s}^{-1}$ . As described by Moura et al. (2009a), the transverse strain was measured in respectively the thickness and width direction of the plate in these two parallel tests, revealing that the transverse deformation is isotropic. Also, it was found that the ratio between transverse and longitudinal strains was not significant different from 0.5 before the longitudinal strain exceeded 1, meaning that the plastic deformation of this PEHD material can be considered as isochoric. Although not shown in Figure 2, tests were also performed in other loading directions than the extrusion direction, but these tests showed that the material essentially can be considered as isotropic.

### 3.2. Dynamic tests

A split-Hopkinson pressure bar was employed to obtain dynamic stress-strain curves in compression. Both bars were 1.5m long and made of PMMA. Further details about the experimental set-up and processing of results are provided by Moura et al. (2009b).

The dynamic compression tests were carried out on ring-shaped specimens with a thickness of 4mm and external and internal diameters of respectively 20mm and 16mm. The strain rates in these tests ranged from 620 to  $4000 \text{ s}^{-1}$ . Figure 2b shows true stress-strain curves from the quasi-static as well as the dynamic compression tests.

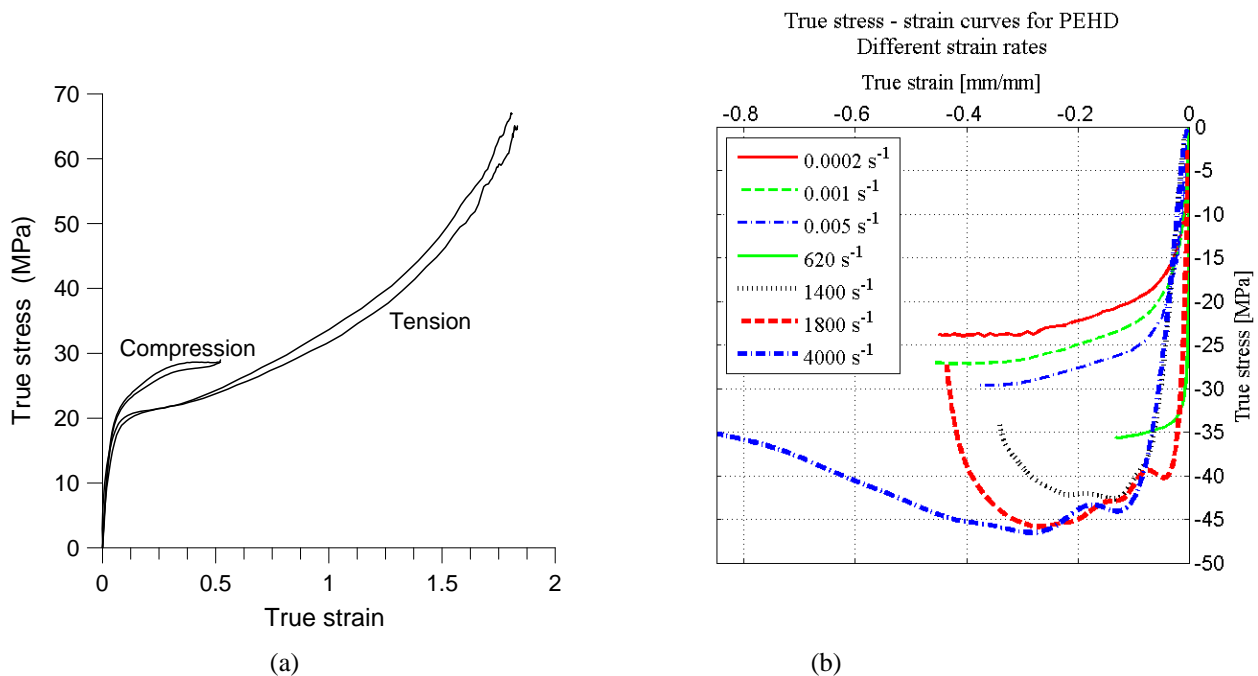


Figure 2. Material tests on PEHD. (a) True stress-strain curves from tension and compression samples tested in the extrusion direction, strain rate  $10^{-3} \text{ s}^{-1}$ . (b) True stress-strain curves from compression samples tested in the extrusion direction at different strain rates (Moura et al., 2009b).

## 4. PARAMETER IDENTIFICATION

The parameters of the constitutive model, see Section 2, were identified from the material tests presented in Section 3. The coefficients are outlined in Table 1. As already noticed, the plastic dilatation of the material was close to zero, therefore,  $\beta = 1$  and effectively a Mises-based flow rule was adopted. Further, the bulk modulus  $\kappa$  was deliberately kept to zero in the calibration procedure, implying a deviatoric stress state in Part B of the model. The coefficients  $E_0$ ,  $\nu_0$ ,  $\sigma_T$ ,  $C_R$  and  $\bar{\lambda}_L$  were determined from a tension test at strain rate  $10^{-3} \text{ s}^{-1}$ . Inverse modeling of the tension test samples was employed to optimize the numerical values. The remaining parameters are justified from the compression tests. Firstly,  $\alpha$  is the ratio between the yield stress in compression and tension. Finally, the rate dependency of the yield stress in compression is fairly well represented by the applied values of  $C$  and  $\dot{\epsilon}_{0A}$ . Also for these parameters, inverse modeling of the tension tests at quasi-static rate was used for an optimization purpose.

Table 1. Calibrated material parameters for the PEHD material.

$E_0$ (MPa)	$\nu_0$	$\sigma_T$ (MPa)	$\alpha$	$\beta$	$\dot{\epsilon}_{0A}$ (s <sup>-1</sup> )	$C$	$C_R$ (MPa)	$\bar{\lambda}_L$	$\kappa$ (MPa)
700	0.48	19	1.267	1.0	0.001	0.0827	2.0	31.62	0

## 5. EXPERIMENTAL TESTS ON PLATES

Quasi-static and dynamic tests were carried out on square PEHD plates with in-plane dimension 600mm x 600mm and thickness 5mm or 10mm. The clamping system was similar in both cases, comprising of two stiff rings holding the plates with 24 M16 bolts along a circle with diameter 500mm. Hence, the tested components were considered as effectively clamped circular plates in the subsequent numerical simulations, see Section 6. The plates were loaded by an impactor in the centre. A cylinder of diameter 60mm and with a rounded end radius of 5mm was used as impactor nose. Moura et al. (2009a) provide further details on the experimental set-up and test results.

Two quasi-static tests were performed in a servo-hydraulic test rig for both thicknesses. A constant speed of 0.1mm/s or 1mm/s was applied in these tests. In general, the plate did not fracture in the quasi-static tests. Instead, the failure mechanism turned out to be an extremely localized deformation of the plate caused by the impactor adjacent to its circumference, see Section 6.

The dynamic tests were carried out in a pneumatic accelerator, where an impactor with total mass of 18.41kg was accelerated by means of pressurized air. The impact velocity varied between 4 and 10m/s. A pair of strain gauges was glued at the impactor immediately above the rounded nose, and the force in the impactor was determined from these gauge registrations. Thus, Newton's second law yields the acceleration of the projectile, and numerical integration provides subsequently the velocity and displacement as function of time. The impact velocity, serving as an initial condition in the integration scheme, was measured by two photo cells.

Four and two dynamic tests, respectively, were carried out on the 5 and 10mm thick plates. The impactor penetrated the plate in two tests, both involving the 5mm thick plate. In the cases without penetration, the plate was globally deformed in a similar way as in the quasi-static tests, but there was no formation of any localized plug.

The main purpose of the test programme was to establish an experimental database for validation of the constitutive model introduced in Section 2. Therefore, determination of the ballistic limit was not an issue in this investigation.

## 6. NUMERICAL SIMULATIONS OF PLATE TESTS

The quasi-static and impact response of the 5 mm thick PEHD plate was investigated with four-node axisymmetric elements in LS-DYNA simulations, involving the constitutive model outlined in Section 2 and the material parameters in Table 1. A reduced integration scheme and hourglass control were applied in the numerical model. The finite element mesh of the circular plate consisted of 8 elements through its thickness and 155 elements along the radius, see Figure 3. Refinement of the mesh did not have any major influence on the results. The steel impactor was assumed as a rigid material with an equivalent density serving to match the mass of 18.41 kg applied in the dynamic experimental tests. Moreover, a frictionless 2D\_automatic\_surface\_to\_surface contact option of LS-DYNA was adopted. The computational time in the quasi-static simulation was reduced by means of mass scaling. It was checked that the kinetic energy was only a small fraction of the total energy.

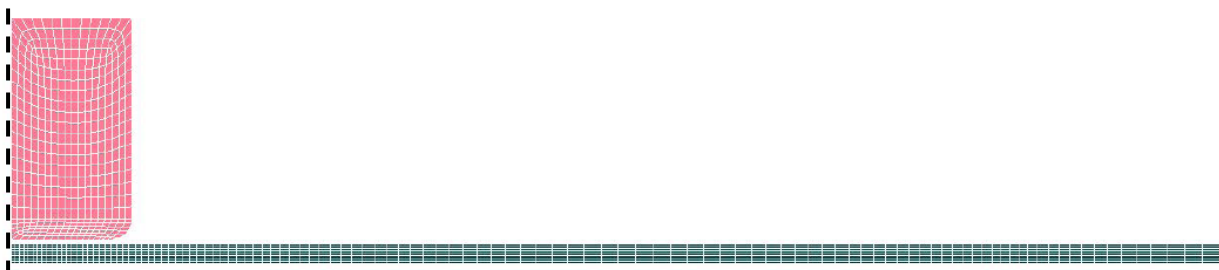


Figure 3. 2D axisymmetric finite element model used in the numerical analyses.

Considering one quasi-static and one dynamic test, force-displacement responses from the experimental tests and numerical simulations are compared in Figure 4. The shape of the curves is fairly well captured in both cases. According to the figure, the numerical analysis underestimates the load-carrying capacity of the plate by about 15 % in the quasi-static case, while the prediction of the dynamic test is excellent. In particular, the different stages in the

experimental test, involving waves going back and forth in the plate and a gradually increasing stiffness, are also found in the force-displacement curve from LS-DYNA.

The shape of the unloading phase is an important issue for several applications of thermoplastic components, e.g. in pedestrian safety assessments. In the dynamic case of Figure 4, the numerical simulation predicts the unloading branch relatively well.

Finally, the quasi-static experimental results suggested that failure was caused by a deep-drawing mechanism forming a localized plug at the centre of the plate. This occurred at a displacement of about 93 mm, see Figure 5a. As illustrated in Figure 5b, this local behaviour is well captured by the numerical model, where the highly localized plastic strain distribution gives an idea of this failure mechanism.

The predictions presented herein must be considered as preliminary results obtained at a rather early stage of research. A more thorough modeling of the boundary conditions and initial plate imperfections (after mounting) may improve the results. Another drawback is that only quasi-static tension tests covering two decades of strain rate were available. The clamping ensures that tension is the most prominent mode during deformation of the plate, and it is not obvious that the rate sensitivity is similar in tension and compression. Further, it is also believed that the observed deviations could have been further clarified with introduction of friction effects in the simulations. Some features of the model may also call for a closer investigation (Polanco-Loria et al., 2009). One potential amendment is to choose another formulation of the non-associated flow rule in the sliding element of Figure 1.

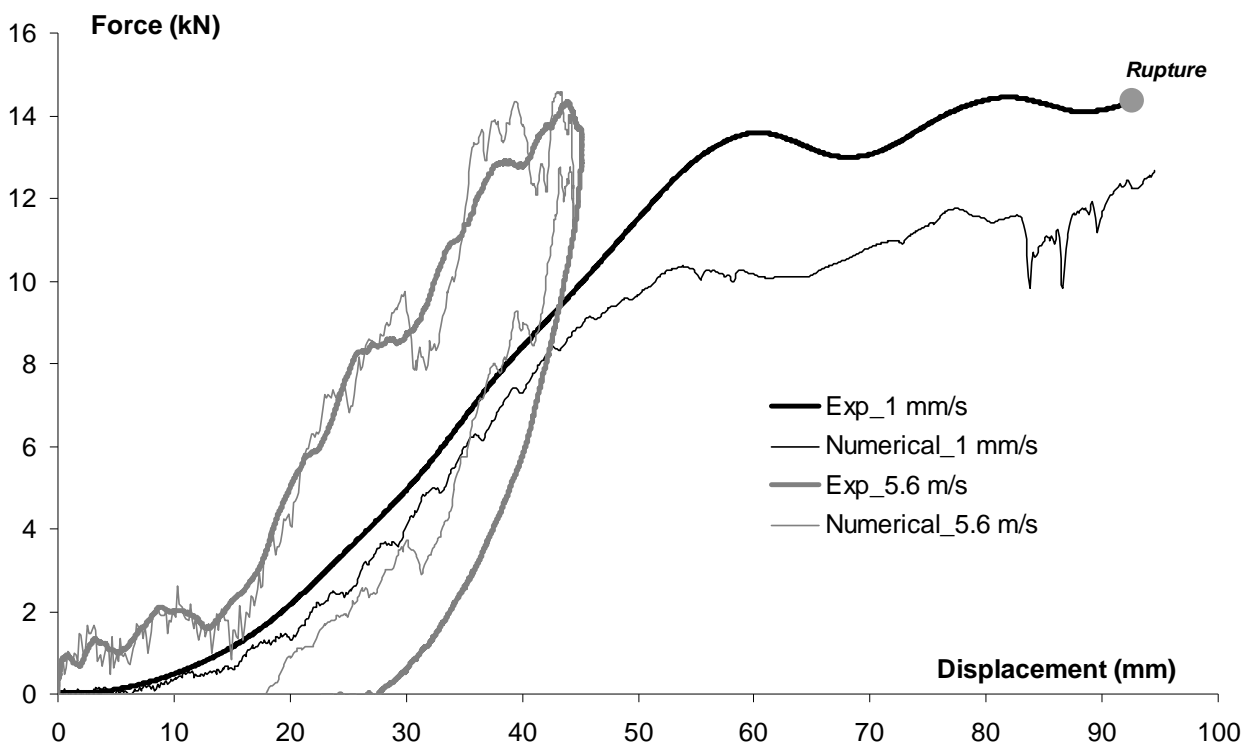


Figure 4. Force-displacement curves obtained in experimental tests and numerical simulations.

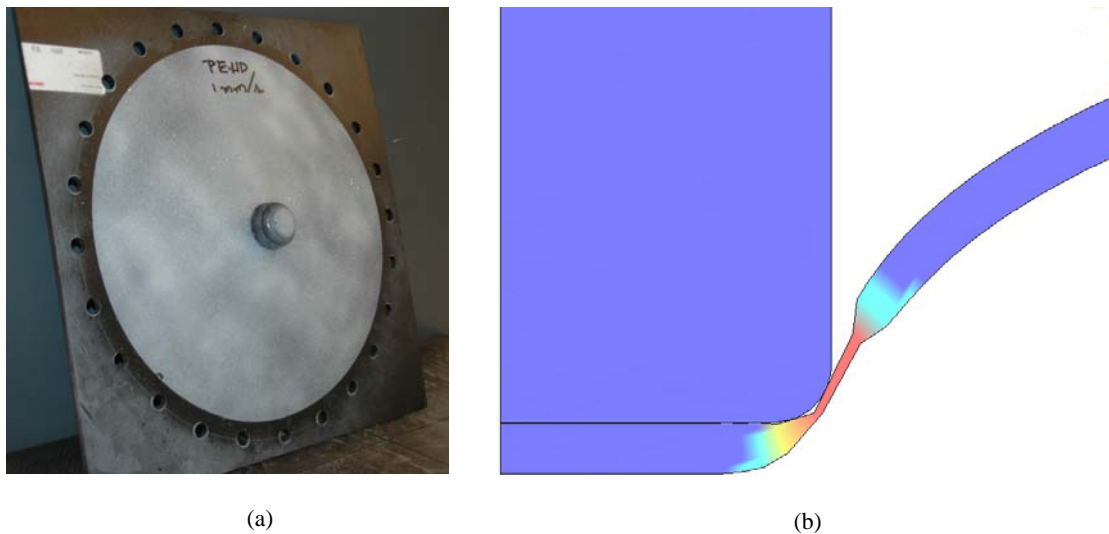


Figure 5. (a) Deformed plate with localized plug after quasi-static testing. (b) Localization around impactor in numerical simulation of a quasi-static test.

## 7. CONCLUDING REMARKS

The constitutive model introduced in Section 2 has been used in numerical simulations of centrally loaded plates made of high-density polyethylene (PEHD). The material model was calibrated from quasi-static uni-axial tests in tension and compression, and dynamic tests in compression. Important features of the experimental observations are captured in the simulations. The force-displacement curve is fairly well represented in the quasi-static case, and the agreement is almost perfect in the dynamic test. Also, the material model is able to describe a cold-drawing effect resulting in a highly localized deformation around the impactor. Although there are uncertainties associated with the material model as well as the numerical modeling of the problem at hand, the results from this rather limited study are promising.

## 8. REFERENCES

- Anand, L., 1996, "A constitutive model for compressible elastomeric solids", *Computational Mechanics*, Vol. 18, pp. 339-355.
- Du Bois, P.A., Kolling, S., Koesters, M. and Frank, T., 2006, "Material behaviour of polymers under impact loading", *International Journal of Impact Engineering*, Vol. 32, pp. 725-740.
- Ehrenstein, G.W., 2001, "Polymeric Materials. Structure – Properties – Applications", Carl Hanser Verlag.
- LS-DYNA, 2007, *Keyword User's Manual*, Version 971, Livermore Software Technology Corporation.
- Moura, R.T., Clausen, A.H., Fagerholt, E., Alves, M. and Langseth M., 2009a, "Impact on PEHD and PVC plates – Experimental tests and numerical simulations", submitted for possible journal publication.
- Moura, R.T., Clausen, A.H., Langseth M. and Alves, M., 2009b, "Dynamic mechanical behaviour of PEHD", accepted for publication in the *European Physical Journal*.
- Polanco-Loria, M., Clausen, A.H., Berstad, T. and Hopperstad, O.S., 2009, "Constitutive model for thermo-plastics with structural applications", submitted for possible journal publication.
- Raghava, R., Caddell, R.M. and Yeh, G.S.Y., 1973, "The macroscopic yield behaviour of polymers", *Journal of Materials Science*, Vol. 8, pp. 225-232.

## 9. RESPONSIBILITY NOTICE

The authors are the only responsible for the printed material included in this paper.